Micromechanical Processes and Failure Phenomena in Reactively Compatibilized Blends of Polyamide 6 and Styrenic Polymers. I. Polyamide 6/Acrylonitrile–Butadiene–Styrene Copolymer Blends

U. A. Handge,[1] C. Sailer,[2] H. Steininger,[3] M. Weber,[4] S. Scholtyssek,[5] V. Seydewitz,[5] G. H. Michler[5]

[1]*Department of Polymer Engineering, Faculty of Engineering Science, Universitätsstrasse 30, D-95447 Bayreuth, Germany*
[2]*Department of Materials, Institute of Polymers, HCI H 530, ETH Zurich, CH-8093 Zurich, Switzerland*
[3]*GKP/R-G201, Polymer Research, BASF SE, D-67056 Ludwigshafen am Rhein, Germany*
[4]*GKT/B-B1, Polymer Research, BASF SE, D-67056 Ludwigshafen am Rhein, Germany*
[5]*Institute of Physics, Martin Luther University of Halle-Wittenberg, D-06099 Halle/S, Germany*

Received 31 July 2008; accepted 25 October 2008
DOI 10.1002/app.29566
Published online 9 February 2009 in Wiley InterScience (www.interscience.wiley.com).

ABSTRACT: In this work, *in situ* investigations of the micromechanical properties of reactively compatibilized blends of polyamide 6 (PA6) and an acrylonitrile–butadiene–styrene copolymer (ABS) were performed with transmission electron microscopy. Three PA6/ABS blends were prepared with a disperse morphology (inclusions of PA6 or ABS) and with a cocontinuous structure. The objective of this work was to study the deformation of the inclusions and the interface between the PA6 phase and the ABS phase. Our transmission electron microscopy investigations revealed that the morphology of the blends was strongly influenced by the asymmetric nature of the interface between PA6 and ABS. In the blends with a PA6 matrix, the interface between PA6 and the ABS inclusions was deformed in tensile deformation under uniaxial loading. A strong influence of the PA6 water content on the (micro)mechanical behavior was observed. Although the "dry" blends behaved in a brittle fashion, the "wet" blends behaved in a ductile fashion with the formation of deformation bands in the matrix (PA6 or ABS), which were initiated by stress concentration at the particles (ABS or PA6, respectively).
 J Appl Polym Sci 112: 1658–1669, 2009

Key words: blends; compatibilization; microdeformation

INTRODUCTION

Multicomponent polymeric materials, such as polymer blends and nanocomposites, are of great technological relevance.[1,2] Blending allows one to combine the favorable properties of different polymers. For example, polyamide 6 (PA6)/acrylonitrile–butadiene–styrene copolymer (ABS) blends are commercially produced for automotive and household applications that require a high impact strength, high chemical resistance, and very good flow properties.[3] Compatibilization of PA6/ABS blends improves the adhesion between the PA6 and ABS phases and enhances the mechanical performance.[4–6] A common compatibilization technique is so-called reactive compatibilization.[7] Here a compatibilization reaction occurs during melt blending, which leads to the formation of graft copolymers at the interface between the PA6 and ABS phases. Generally, the exact amount of formed compatibilizer molecules is unknown, and this complicates investigations of the influence of reactive compatibilization on the blend properties. Consequently, a large number of attempts have been undertaken to achieve a complete understanding of the morphological, mechanical, and rheological properties of reactively compatibilized PA6/ABS blends.

A series of previous studies focused on the mechanical and rheological properties of reactively compatibilized blends of PA6 and styrenic polymers.[8–13] Jafari et al.[9] studied the thermal behavior and morphology of PA6 blends with styrenic polymers. Their study revealed that compatibilized blends had a lower nucleation rate in the PA6 phase than uncompatibilized ones. The evolution of the morphology in PA6/styrene–acrylonitrile copolymer (SAN) blends with a PA6 matrix that were compatibilized with a reactive imidized acrylic polymer

Correspondence to: U. A. Handge (ulrich.handge@uni-bayreuth.de).
Contract grant sponsor: Swiss National Science Foundation (to C.S. and U.A.H.); contract grant number: 200021-103287.
Contract grant sponsor: International Union of Pure and Applied Chemistry (to Chairman H.S.T.); contract grant number: 2005-023-2-400.

during extrusion was studied by Majumdar et al.[10] In the initial part of the extruder screw, the particle size decreased with the compatibilizer concentration, whereas in the latter stage, coalescence of the dispersed particles was pronounced.[10] Morphological investigations of PA6/SAN blends with additional styrene copolymers have revealed that an optimum concentration of maleic anhydride in the styrene copolymers exists that leads to a minimum particle size.[11] The detection of cocontinuous structures in PA6/SAN blends with different methods was discussed by Pötschke and Paul.[12] Furthermore, Lee et al.[13] investigated the dependence of the morphology of PA6/ABS blends on the composition, compatibilizer concentration, and feed rate. Their analysis showed that the viscosity ratio and the compatibilizer concentration strongly influenced the average size of the dispersed domains. In particular, a maximum of the mean particle size as a function of the feed rate was observed.

Paul et al.[14] intensively studied the mechanical and processing properties of PA6/SAN blends (see their work for an introduction). The phase inversion behavior and the size of the dispersed particles of reactively compatibilized PA6/SAN blends were investigated by Kitayama et al.[15,16] The morphological analysis indicated a strong (imidized acrylic polymer as a compatibilizer) or weak (styrene–acrylonitrile–maleic anhydride terpolymer as a compatibilizer) asymmetric situation depending on whether PA6 or SAN forms the matrix.[15,16] A main result of the tensile stress–strain studies by Kitayama et al.[17] was that a possible relationship between the size of SAN particles and plastic deformation exists. The mechanical properties and morphology of PA6/ABS blends that were compatibilized with imidized acrylic polymers were the subject of a study by Majumdar et al.[18] In this work, the PA6/ABS blends with the most uniform dispersion of ABS particles led to the lowest brittle–ductile transition temperature and to the maximum Young's modulus. The deformation mechanism during the fracture of PA6/ABS blends was also studied by Majumdar et al.[19] The cavitation of the rubber particles in compatibilized blends and the subsequent shear yielding of the PA6 matrix caused high toughness values. Related studies using PA6 and styrenic blends were performed by Janik et al.[20] and Steenbrink et al.[21] In a study by Majumdar et al.,[22] the morphology of PA6/ABS blends that were compatibilized by a styrene/maleic anhydride copolymer was investigated as a function of the copolymer concentration. Increasing the weight fraction of the copolymer led to an improved dispersion of the ABS domains. The concept of the essential work of fracture was applied by Pressly et al.[23] to study the temperature dependence of the fracture properties of PA6/ABS blends. With this concept, the mechanical parameters in brittle, ductile, and mixed-mode fracture as a function of temperature were determined. A decrease in the temperature also decreased the amount of plastic deformation at the notch. Finally, a systematic analysis of the morphological and mechanical properties of compatibilized PA6/ABS blends was performed by Araújo et al.[24,25] In summary, the influence of reactive compatibilization on the macroscopic properties of blends of PA6 and styrenic polymers has been studied for a variety of different systems. However, the microscopic failure mechanisms during tensile deformation based on *in situ* investigations have been explored to a much lesser extent.

Recently, the influence of reactive compatibilization on the rheological properties of PA6/SAN blends with different types of morphology has been investigated.[26–28] These works have revealed that reactive compatibilization tremendously influences the complex modulus, extensional viscosity, and recoverable deformation of PA6/SAN blends. In particular, the asymmetric properties of the interface between PA6 and the styrenic phase have been demonstrated by morphological studies and linear viscoelastic shear oscillations.

In this study, we investigated the mechanical and rheological properties of reactively compatibilized PA6/SAN and PA6/ABS blends. Although previous works mostly were devoted to macroscopic investigations or a microscopic analysis of fractured samples, the objective of this work was to analyze the micromechanical mechanisms that take place during the tensile deformation of the blends. Therefore, micromechanical tests of ultrathin sections of the blends were performed with transmission electron microscopy (TEM). Through the variation of the PA6 content, blends with different types of morphology were studied. Because the deformation behavior of PA6 depends on the moisture content of the samples, the mechanical tests were performed in dry and wet states. This article reports on the first part of this study and summarizes the results for the PA6/ABS blends (part I). Part II presents the results for the PA6/SAN blends.

EXPERIMENTAL

Materials

Blends of PA6 (Ultramid B4®) and ABS with an acrylonitrile content of 35 wt % were prepared. The blend components were provided by BASF SE (Ludwigshafen am Rhein, Germany; see Table I for the physical properties of the blend components). The rubber content in the ABS phase was 10 wt %, and the diameter of the rubber particles ranged between 40 and 90 nm, with a small fraction of particles

TABLE I
Physical Properties of PA6 and SAN Used for the Preparation of ABS

	T_g (°C)	T_m (°C)	M_n (g/mol)	M_w (g/mol)	M_w/M_n	η_0 at 240°C (Pa s)
PA6	53	221	23,000	121,000	5.3	8,400
SAN	109	—	57,800	150,000	2.6	2,400

ABS was composed of SAN and 10 wt % rubber and also included 6.8 wt % SANMA. η_0 = zero-shear-rate viscosity; M_n = number-average molecular weight; M_w = weight-average molecular weight; T_g = glass-transition temperature; T_m = melting temperature.

having a diameter up to 140 nm. A styrene–acrylonitrile–maleic anhydride random terpolymer (SANMA) was added to the ABS grade. The weight fraction of SANMA was 6.8 wt % in the ABS grade. The terpolymer SANMA was composed of 2 wt % maleic anhydride, 29 wt % acrylonitrile, and 69 wt % styrene and had a weight-average molecular weight of 115,000 g/mol and a number-average molecular weight of 52,000 g/mol. On average, approximately 20 maleic anhydride groups were randomly located on the backbone of one SANMA chain.

We prepared three PA6/ABS blends by melt extrusion. First, granules of the blend components were premixed and dried *in vacuo* at 80°C for 7 days. Then, melt blending was performed with a corotating twin screw extruder (Brabender, Duisburg, Germany). The diameter of the screws was 25 mm, and the length/diameter ratio was 22. The extrusion temperature was 240°C, and the speed of the screws was 50 rpm. The weight fraction of PA6 was 30, 50, or 70% (see Table II). The single components were extruded under the same conditions used for the blends. After the melt had left the die of the extruder, the extrudate was piled up to compact objects of roughly 250 g. After solidification, these extruded specimens were cut into bodies with parallel surfaces. Then, these cut extrudates were compression-molded into plates with dimensions of $4 \times 130 \times 150$ mm^3 at 240°C for 30 min *in vacuo*. The samples for the rheological experiments were milled from compression-molded plates with dimensions of $2 \times 70 \times 100$ mm^3 (30 min of compression molding at 240°C).

In the initial stage of extrusion, the maleic anhydride groups of the SANMA chains reacted with the amino end groups of PA6 and formed SAN-*graft*-PA6 copolymers (see Fig. 1). Previous studies have shown that the compatibilization reaction proceeds very rapidly in the early stage of mixing.[3,10,29] The graft copolymers that were formed during melt mixing were preferentially located at the interface between the PA6 and the ABS phases and improved the interfacial adhesion between the two phases in the solid state. Note that the SANMA concentration in the ABS grade was constant. Therefore, the concentration of SANMA in each blend varied with the ABS concentration. However, the probability that a graft copolymer was formed at the interface between PA6 and ABS was roughly equal for all blends.

Rheological experiments

Before the rheological experiments were started, the samples were stored and shielded from light *in vacuo* at 80°C for at least 7 days. The linear viscoelastic properties of the blend components (PA6 and ABS) and the PA6/ABS blends were probed with harmonic shear oscillations at 240°C. A UDS 200 universal dynamic spectrometer (Physica, Stuttgart, Germany) with a plate–plate geometry was used. The plate diameter was 25 mm, and the gap was 1.8 mm. Amplitude and time sweeps were carried out to determine the linear viscoelastic range and the thermal stability of the melts. Then, frequency sweeps were performed in the range of $0.025 \text{ rad/s} \leq \omega \leq 396 \text{ rad/s}$, where ω is the angular frequency. The shear amplitude was set to $\gamma_0 = 0.03$. All rheological experiments were performed in a nitrogen atmosphere.

TABLE II
Compositions and Fracture Mechanisms of the Reactively Compatibilized PA6/ABS Blends

	PA6 (wt %)	ABS (wt %)	SANMA (wt %)	Fracture mechanism
PA6	100.0	0.0	0.0	Necking
70% PA6/30% ABS	70.0	28.0	2.0	Brittle
50% PA6/50% ABS	50.0	46.6	3.4	Stress whitening
30% PA6/70% ABS	30.0	65.2	4.8	Stress whitening
ABS	0.0	93.2	6.8	Stress whitening

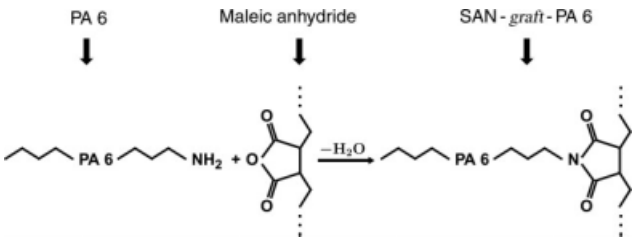

Figure 1 Scheme of the compatibilizing reaction between the maleic anhydride groups of SANMA and the amino end groups of PA6.

Mechanical experiments

The specimens for the mechanical tests were shaped according to ISO standard 527-2/1BA. The specimens were dried for 7 days at 80°C *in vacuo* and annealed before testing for 1 h at 90°C in a N_2 atmosphere (for the measurements in the dry state). The environmental conditions during testing were 23°C and a relative humidity of 50%. The experiments were performed with a crosshead velocity of 1 mm/min for the measurement of the Young's modulus and 5 mm/min for the measurement of the nominal maximum stress, yield stress, and elongation at break.

Morphological analysis

The specimens for the morphological and micromechanical analyses were prepared with ultramicrotomy. To study the morphology of the materials, the first step of preparation was cutting the sheets into small pieces (ca. $10 \times 5 \times 5$ mm^3). Then, a flat surface was trimmed with a diamond knife. These samples were stained in a solution of osmium and formalin for 1 week at 60°C. After staining, the specimens were dried at 60°C for 3 days. The last step was thin sectioning of the samples at room temperature by means of an ultramicrotome equipped with a 35° diamond knife. The thickness of the sections was 80 nm. After the ultrathin sections were transferred into the specimen holder for the transmission electron microscope, the TEM investigations were performed with a Leo 912 transmission electron microscope (Zeiss, Oberkochen, Germany) operated at a 120-kV acceleration voltage in the zero-loss-electron mode.

Micromechanical analysis

For the micromechanical analysis, semithin sections approximately 1 μm thick, several millimeter long, and 0.5 mm wide were prepared with an ultramicrotome. These samples were positioned in a special microtensile apparatus of the transmission electron microscope. The different mechanical behaviors of wet and dry PA6 led to micromechanical investigations of dry and wet specimens with two different approaches for preparation. The wet situation was simulated by the application of a water droplet onto the semithin section before straining, whereas the deformation of the dry specimen took place *in situ* in the transmission electron microscope (i.e., *in vacuo*) by means of a special tensile stage. Because of the thickness of the specimen, a JEM 4000 FX microscope (JEOL, Ltd., Tokyo, Japan) with an acceleration voltage of 400 kV was used for these investigations (in cooperation with the Max Planck Institute of Microstructure Physics, Halle/S, Germany). Details of the micromechanical techniques are described by Michler et al.[30,31]

RESULTS

Linear viscoelastic shear oscillations

The results of the linear viscoelastic shear oscillations at 240°C are presented in Figure 2. The storage modulus (G') and loss modulus (G'') of neat PA6 attained a shape that is typical for a polydisperse thermoplastic polymer [see Fig. 2(a,b)]. Both G' and G'' decreased with ω decreasing. At large values of ω, G' was larger than G''. On the contrary, at low values of ω, we found $G'' \gg G'$, and so the loss tangent (tan δ) was larger than [see Fig. 2(c)]. In the low frequency range, the complex modulus of PA6 almost attained the terminal behavior of the Maxwell element (a spring in series with a dashpot), which is given by $G' \propto \omega^2$ and $G'' \propto \omega$. Extrapolating the complex viscosity, $|\eta^*(\omega)| = \sqrt{G'^2 + G''^2}/\omega$, to $\omega \to 0$ led to the zero-shear-rate viscosity (8400 Pa s) for PA6 at 240°C.

At large values of ω, ABS behaved similarly to PA6. In the range of large frequencies, the elasticity caused by the physical entanglements mostly determined the viscoelastic response. At low values of ω, G' of ABS did not obey the power law $G' \propto \omega^2$, in contrast to neat PA6. Furthermore, tan δ as a function of ω attained a maximum and decreased with lower values of ω at low frequencies; see also Masuda et al.[32] and Aoki.[33] This tendency indicated an increase in elasticity at low stresses and was caused by the elastic interactions between the rubber particles.

G' and G'' of all PA6/ABS blends exceeded the corresponding values of pure PA6 and pure ABS [see Fig. 2(a,b)]. Reactive compatibilization led to the synthesis of multigraft copolymers and thus increased the viscous and elastic properties of the blend components. The loss tangent tan δ as a function of ω revealed that for the blends with 30 or 50% PA6, elastic interactions were strongly pronounced at low values of ω [see Fig. 2(c)]. In this case, tan δ

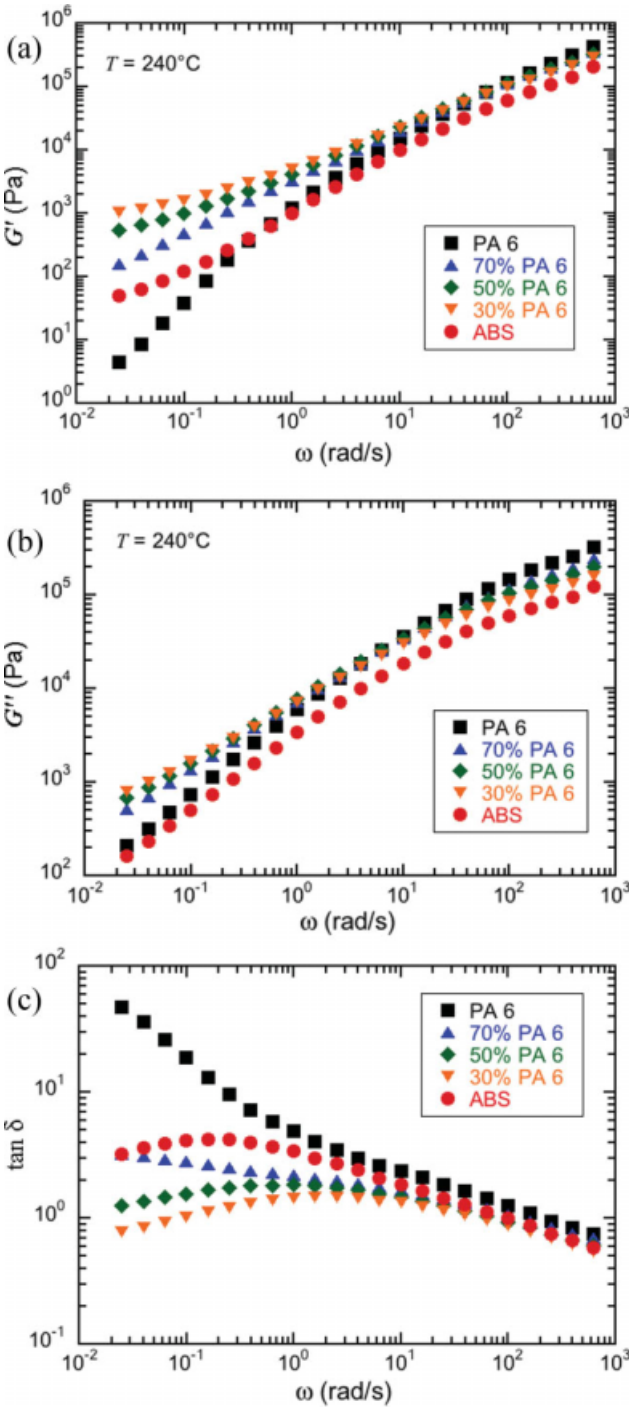

Figure 2 (a) G', (b) G'', and (c) tan δ (G''/G') as a function of ω at 240°C for PA6, ABS, and the three PA6/ABS blends. The weight fractions of PA6 and ABS are indicated. [Color figure can be viewed in the online issue, which is available at www.interscience.wiley.com.]

attained a maximum, and at low values of ω, the relation tan $\delta < 1$ held for the blend with 70% ABS. PA6 formed the matrix phase in the 70% PA6/30% ABS blend. This blend depicted a behavior that did not differ much from the power laws $G' \propto \omega^{1/2}$ and $G'' \propto \omega^{1/2}$; see also Sailer and Handge.[28] This relaxation pattern was caused by the large number of micellelike domains in the PA6 matrix (vide infra) and can be explained by cooperative relaxation processes of the multigrafted copolymers; see Sailer and Handge for a detailed discussion.

Mechanical experiments

The stress–strain diagrams of the neat blend components and the PA6/ABS blends are presented in Figure 3. Before the beginning of the mechanical tests, the materials were strongly dried. Therefore, all macroscopic mechanical tests refer to the so-called dry state. Pure PA6 behaves in a ductile fashion. The neat ABS grade revealed a marked yield point and an elongation at break of about 23%. The characteristic mechanical properties are shown in Figure 4. With increasing PA6 content in the PA6/ABS blends, the Young's modulus slightly increased, the yield stress and maximum stress increased clearly, but the elongation at break was very low. The elongation at break values of both blend components were much larger than the corresponding values of the PA6/ABS blends.

Morphological investigations

The morphology of ABS, PA6, and the three PA6/ABS blends after compression molding is presented in Figures 5–8. Figures 5(a,b) depicts the typical morphology of an ABS copolymer. The weight fraction of the rubber particles was 10 wt %, which was a very moderate value in comparison with commercial grades of ABS. The rubber particles were uniformly dispersed in the SAN matrix. The diameter of the particles ranged from 40 to 90 nm. A small number of rubber particles had a diameter up to

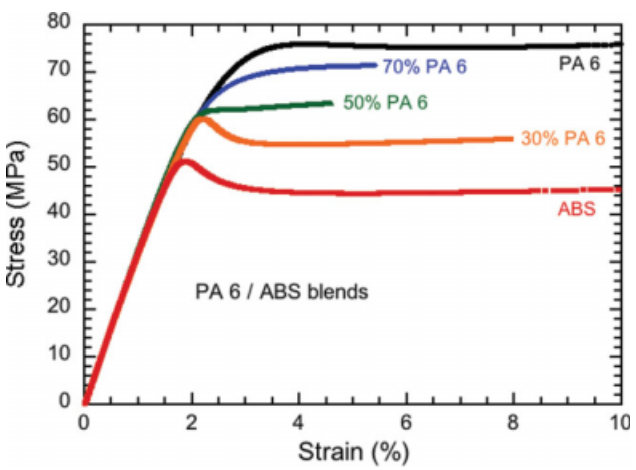

Figure 3 Nominal stress versus strain for PA6, ABS, and the PA6/ABS blends in the dry state. [Color figure can be viewed in the online issue, which is available at www.interscience.wiley.com.]

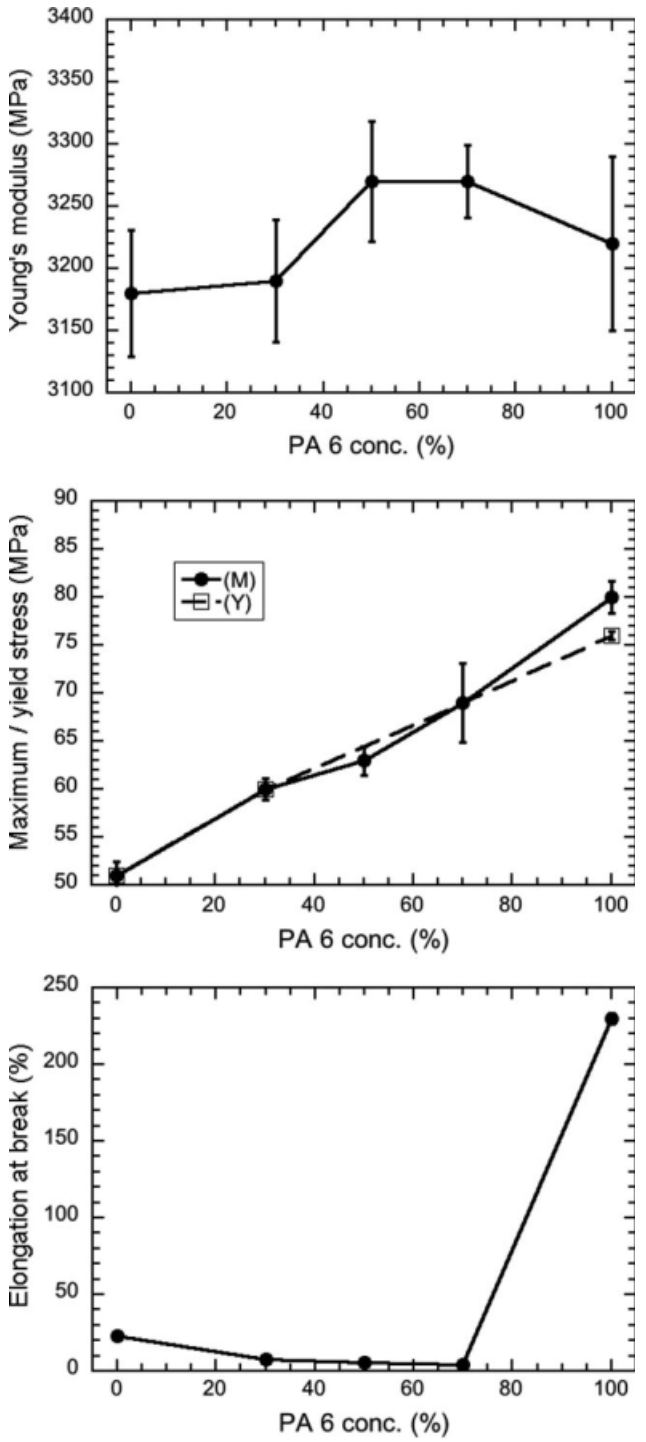

Figure 4 Mechanical properties of the PA6/ABS blends at room temperature: (a) Young's modulus, (b) maximum stress and yield stress, and (c) elongation at break.

140 nm. Because of the grafting of SAN macromolecules onto the surface and inside the rubber particles, the particles revealed a rough surface structure and small bright dots inside (SAN subinclusions up to 10–20 nm in size). The neat PA6 polymer showed a dendritic morphology with a pronounced parallel arrangement of the lamellae [see Fig. 5(c,d)].

The PA6/ABS blends formed multiphase structures. Figures 6(a,b) presents the disperse morphology of the 30% PA6/70% ABS blend with PA6 domains in the ABS matrix. The average size of the PA6 particles ranged from half a micrometer to some micrometers. Some particles were aggregated, but the interface between these neighbored particles could still be seen. The particles were elliptically to irregularly shaped. The particles revealed the semicrystalline morphology of PA6 with lamellae, which were relatively short and about 10 nm thick. Inside the PA6 particles, small, bright domains up to 50 nm in diameter were visible, arising probably from the compatibilizer SANMA. The rubber particles of the ABS phase were preferentially located near the PA6/SAN interface, which corresponded to an energetic minimum. In many cases, the distances between the rubber particles and the PA6 particles were in the range of 20 nm [cf. Fig. 6(b)]. These distances could probably be correlated with the SAN grafting layer at the rubber.

After compression molding, the domains of the 50% PA6/50% ABS blend formed a cocontinuous structure [see Fig. 7(a,b)]. The average size of the domains of the cocontinuous structure was much larger than the mean size of the domains of the blends with 70 and 30% ABS, respectively. The average free length in both phases was in the range of a few micrometers. Inside the PA6 particles, small subinclusions about 50 nm in size were visible. These micellelike objects most likely were highly compatibilized SAN domains or PA6-grafted SANMA terpolymers (cf. Sailer and Handge[28]).

Finally, the 70% PA6/30% ABS blend consisted of ABS domains that were uniformly dispersed in the continuous PA6 matrix and about 0.5–2 μm in size [cf. Fig. 8(a,b)]. In addition, a huge number of very small ABS particles with a diameter smaller than 500 nm were located in the PA6 matrix. These very small ABS particles contained only a few or no rubber particles. Larger ABS particles exhibited a large number of rubber particles, which were predominantly located near the interface and partially clustered. The rubber particles did not seem to have a strong influence on the morphology because their weight concentration was 10 wt % and thus they had only a small influence on the viscosity at the shear rates of extrusion. Inside the PA6 matrix, the lamellar semicrystalline morphology was visible.

Micromechanical analysis in TEM

In this study, *in situ* investigations of semithin sections of the blends with a disperse and cocontinuous morphology (30, 50, and 70% weight fraction of PA6) were performed under uniaxial loading with TEM. This technique has also been applied to other

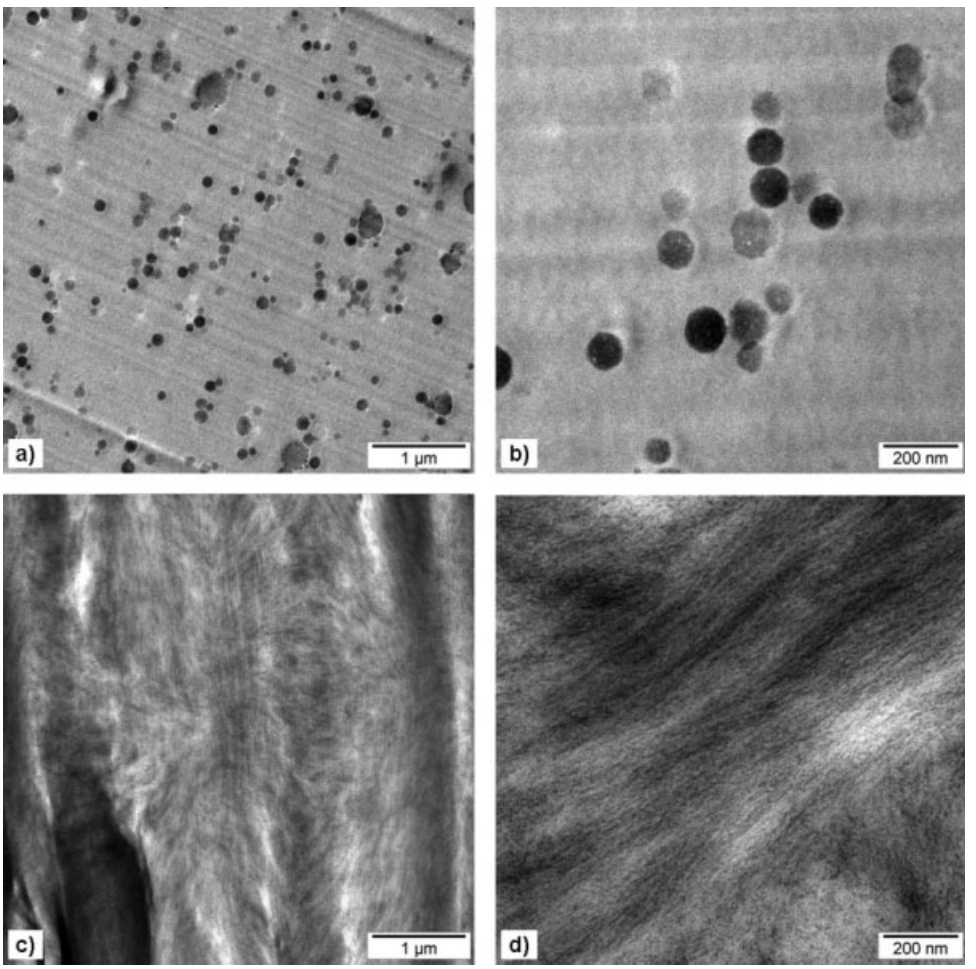

Figure 5 Morphology of the blend components at lower and higher magnifications: (a,b) ABS and (c,d) PA6.

polymer blends.[34] The micromechanical analysis of the compression-molded samples was performed in the described way for investigating the impact of absorbed water. In the following, the water content of PA6 is denoted by the terms *wet* and *dry*.

The micromechanical investigations by 400-kV TEM of neat PA6 showed homogeneous deformation without any fibrillation, cavitation, or crazing in the wet and dry states. The samples of the 30% PA6/70% ABS blend in the wet state showed a stretching

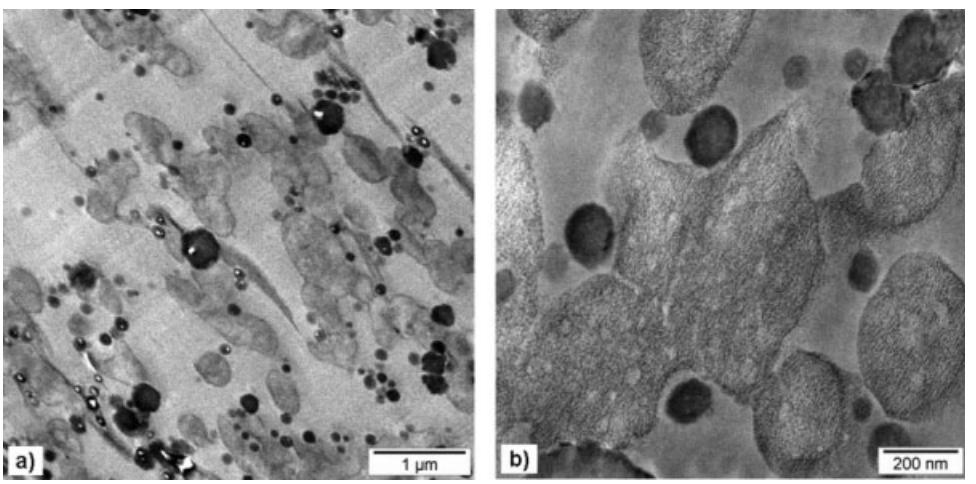

Figure 6 Morphology (phase structure) of a selectively stained ultrathin section of the 30% PA6/70% ABS blend obtained by TEM: (a) lower magnification and (b) higher magnification.

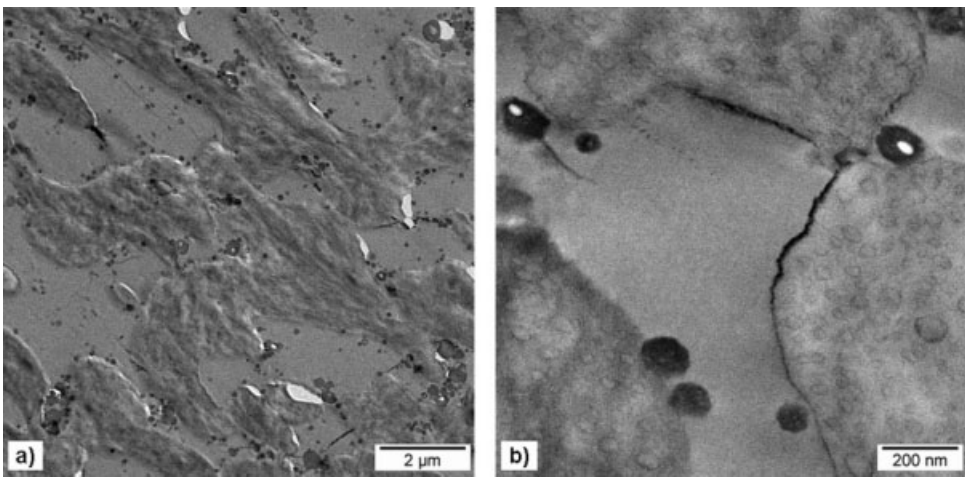

Figure 7 TEM micrographs of the 50% PA6/50% ABS blend: (a) lower magnification and (b) higher magnification of a selectively stained ultrathin section.

of the ABS matrix with deformed elastomer particles and localized deformation bands between them [see Fig. 9(a–c)]. The particles, which behaved like elastomeric ones and had diameters between approximately 100 nm and a few micrometers, were PA6 particles. In the wet state, they were rubberlike, acted as stress concentrators, and initiated plastic deformation of the ABS matrix. The deformation bands in the ABS matrix between the PA6 particles contained homogeneous plastic yielding as well as fibrillated crazes, both typical deformation mechanisms of ABS and SAN. However, this deformation pattern was coarser than the usual deformation pattern of ABS around rubber particles (thin homogeneous or fibrillated crazes ca. 100-nm in size[35]). This deformation mechanism could extend across large volumes of the sample. However, large PA6 particles could cavitate, creating voids, and therefore initiate crack propagation. The corresponding dry sample showed brittle fracture. In zones of higher stresses near crack tips, larger PA6 particles appeared brighter, and this indicated that they were somewhat stretched [Fig. 9(d)], but with only a very low stress concentration and nearly no initiation of plastic deformation in the ABS matrix [Fig. 9(e)].

Generally, the samples in the dry state behaved more brittlely under tensile deformation than the specimens in the wet state. The 50/50 PA6/ABS sample in the wet state also showed a banded deformation pattern (Fig. 10), but the deformed PA6 particles were not so numerous and not so clearly visible as in the former material. There were more diffuse deformation bands with larger undeformed areas between them. The deformation pattern was developed only in the ABS areas and was more structureless in the PA6 areas. The fibrillated crazes were relatively thin [Fig. 10(b)].

In the 70% PA6/30% ABS sample, the deformation mechanism was changed (see Fig. 11 for the wet

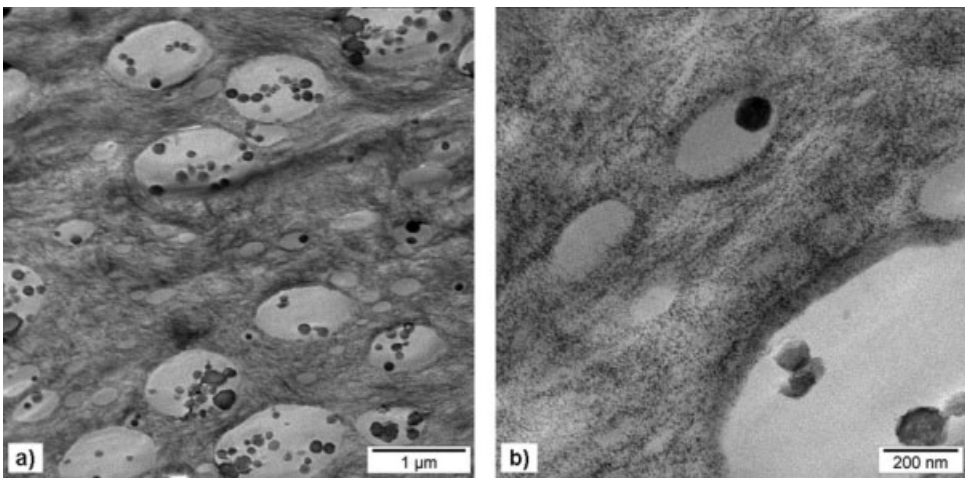

Figure 8 Morphology (phase structure) of the 70% PA6/30% ABS blend: (a) lower magnification and (b) higher magnification of a selectively stained ultrathin section (TEM micrograph).

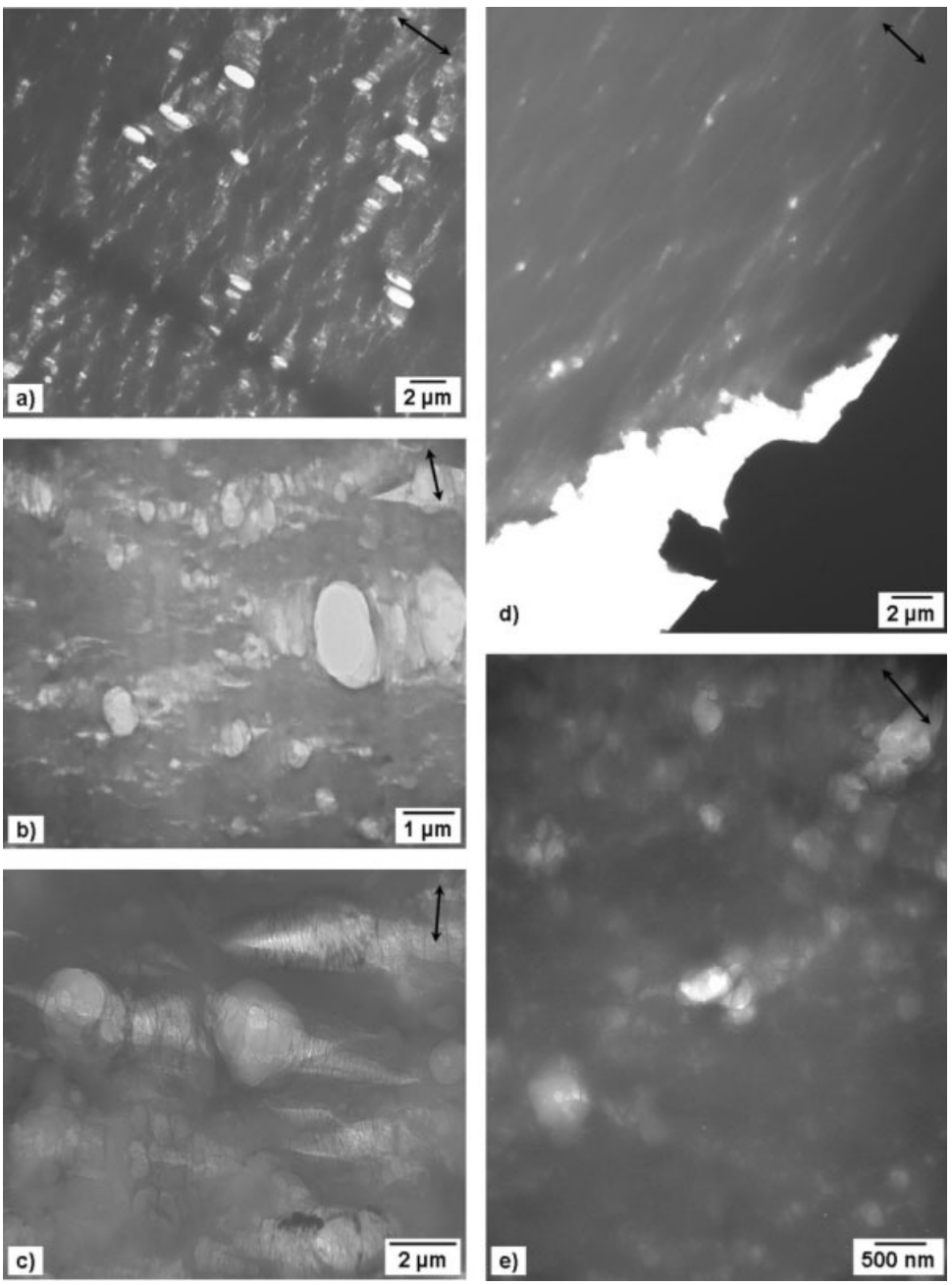

Figure 9 Deformation structures (TEM micrographs) of the 30% PA6/70% ABS blend: (a–c) deformation in the wet state and (d,e) deformation in the dry state. The arrows indicate the loading direction.

state). The ABS particles, about 0.5–2 μm in diameter, were debonded from the PA6 matrix without any plastic deformation themselves. The voids around the ABS particles were elongated up to several hundred percent, and this indicated high local ductility of the PA6 matrix. The pattern of elongated voids was concentrated at places where the largest ABS particles or a concentration of larger particles appeared. If the distance between the elongated voids, that is, the thickness of the deformed PA6 strands, was too small, the voids could coalesce and produce a crack. The interface between the ABS particles and PA6 matrix often was smooth but partially fibrillated, and this indicated locally better adhesion or a special interphase [Fig. 11(b)].

DISCUSSION

The morphology of the PA6/ABS blends was strongly influenced by the composition and the formation of the graft copolymer. In two-phase equiviscous polymer blends, the major phase generally tends to form the matrix phase. Thus, the blends with 30 and 70% PA6 had a disperse morphology.

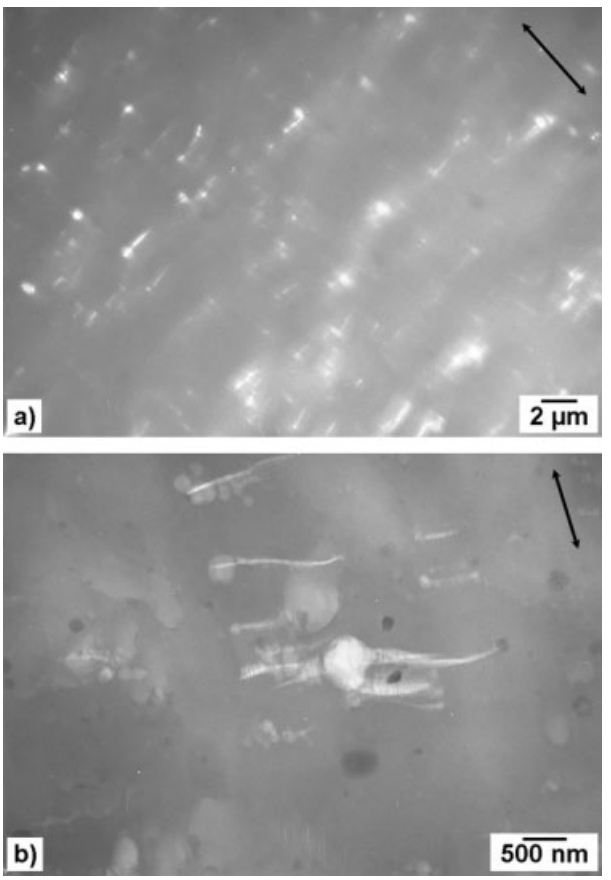

Figure 10 Deformation structures (TEM micrographs) of the 50% PA6/50% ABS blend in the wet state: (a) low magnification and (b) high magnification. The arrows indicate the loading direction.

In the case of the PA6 matrix, spherical ABS drops were embedded in the continuous PA6 matrix. The chains of the SAN-*graft*-PA6 copolymer were located at the interface between PA6 and the styrenic phase, so the interface was compatibilized. If the compatibilizer molecules had not been present at the interface, the morphology would have become coarse-grained during compression molding and the ABS domains would have been much larger in size. Furthermore, small, highly compatibilized SAN drops were also located in the PA6 phase. These small inclusions were stable only in the PA6 matrix and not in the ABS phase. After extrusion of the blends with 30% PA6 and 50% PA6, the PA6 domains were uniformly dispersed in the ABS matrix. In contrast to the blend with 70% PA6, the morphology of these blends changed during compression molding (cf. Sailer and Handge[26]). The PA6 domains tended to aggregate, and this led to a cocontinuous structure for the blend with 50% PA6 and to aggregated PA6 domains for the blend with 30% PA6. In conclusion, the stability of the morphology was strongly influenced by the interfacial properties. The morphology of the blends with 70% PA6 was stable, whereas for the blends with 30% PA6 and 50% PA6, aggregation and partial coalescence were observed. This experimental observation indicated an asymmetric nature of the interface between PA6 and the styrenic component. Consequently, the interaction between the domains of the disperse phase depended on the matrix phase (PA6 or styrenic component).

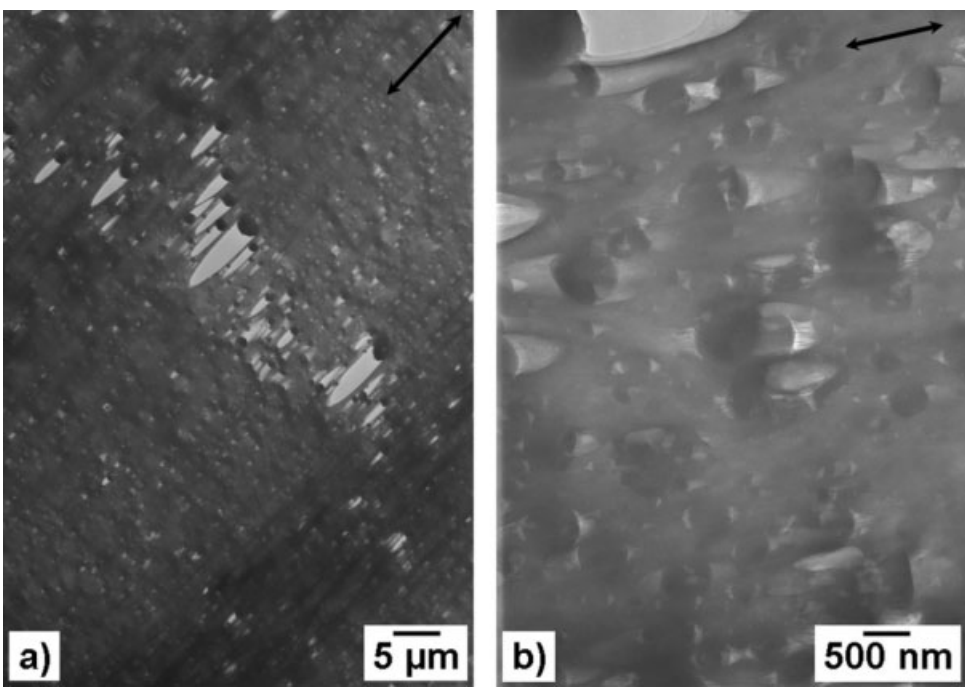

Figure 11 Deformation structures (TEM micrographs) of the 70% PA6/30% ABS blend in the wet state: (a) overview and (b) higher magnification. The arrows indicate the loading direction.

Figure 2 reveals that in the range of low frequencies, G' and G'' of all blends were much larger than the moduli of the neat materials. This experimental result indicates that the reactive compatibilization led to the synthesis of high-molecular-weight copolymers that were associated with a high viscosity. The blend with a PA6 matrix showed a power-law relation for G' and G''. The relaxation of the graft copolymers was so strongly pronounced that the influence of the rubber particles in the 70% PA6/30% ABS blends was masked at low values of ω. On the other hand, the blend with an ABS matrix tended to plateau in the low frequency range. This different rheological behavior for the blends with 30 and 70% PA6 also indicated asymmetric interfacial properties between PA6 and ABS.

The mechanical behavior of the neat components ABS and PA6 corresponded with the usual, well-known behavior of an ABS with a lower rubber content (10 wt %) and a PA6. However, all the blends (in the dry state) showed a loss of ductility and a reduction of the elongation at break. There was no change in Young's modulus (ca. 3200 MPa), but there was a steady increase in the yield stress from 51 (for ABS) to 76 MPa (for PA6). The brittleness (low elongation at break of ca. 4–8%) of the blends corresponded with the micromechanical deformation behavior of the sample deformed in the dry state [30% PA6/70% ABS; see Fig. 9(d,e)]. The PA6 particles under dry conditions behaved relatively stiffly up to larger stresses and were unable to initiate plastic deformation in the ABS matrix. The larger PA6 particles ruptured into microvoids and created the path for brittle crack propagation.

The same morphology deformed under wet conditions showed a very different behavior. In this case, the PA6 particles behaved in a ductile fashion and (because they were softer than the matrix) acted as stress concentrators. In the stress concentration zones, the adjacent parts of the ABS matrix were plastically deformed with typical homogeneous deformation zones and fibrillated crazes [Fig. 9(a–c)]. Hence, the change in the 30% PA6 due to the water content modified the deformation mechanism.

The wet samples of the 50% PA/50% ABS blend showed behavior similar to that of the former wet blend. The PA6 particles acted as soft stress concentrators and initiated homogeneous deformation bands in the interconnected ABS parts. Because of the interconnected phase structure, the deformation bands were more diffuse.

The wet 70% PA6/30% ABS blend showed very different micromechanical behavior. The SANMA concentration was only 2.0 wt % for this blend (see Table II). Consequently, the ABS particles revealed only limited interfacial strength, which resulted in debonding and microvoid formation around particles under load (Fig. 11). The ABS particles themselves were not deformed, but the PA6 matrix strands between the elongated microvoids showed large plastic deformation (deformed in the wet state). From the enlargement of the microvoids, plastic deformation of the PA6 strands of more than 300% could be estimated, and this value is larger than the elongation at break of PA6 in the bulk. The deformation in the PA6 matrix strands appeared to be homogeneous. Because of the limited interfacial strength, debonding (void formation) appeared before yielding of the ABS particles could occur. That means that the interfacial strength was lower than the yield stress of ABS (ca. 50 MPa). In general, the combination of micromechanical properties revealed by TEM and macroscopic stress–elongation tests can give values of the interfacial strength or adhesion force: The appearance of microvoids around ABS particles in TEM correlates with the first deviation of the stress–elongation curve from the straight line in the macromechanical test.

The brittle behavior of the blends under dry conditions (elongation at break between 4 and 8%) was the result of a reduction of the ductility of the PA6 component. Because the macromechanical testing was performed with very dry samples, it is expected that materials with a distinct deformation pattern will reveal better ductility and greater elongation at break under environmental conditions, that is, with a higher water content.

CONCLUSIONS

In this study, the morphology and mechanical properties of reactively compatibilized PA6/ABS blends were investigated. To study the micromechanical deformation processes, investigations of thin sections of these blends were performed with TEM. Because the mechanical properties of PA6 strongly depend on its water content, the experiments were performed in wet and dry states. The analysis of our experiments led to the following conclusions.

First, the morphology of the PA6/ABS blends followed the general mixing rule with an increasing content of PA6: spherical particles, interconnected network, and matrix. The low rubber content (10 wt %) in the ABS phase mainly influenced the flow properties at low shear rates, but not at shear rates that are typical for extrusion. In the blends with 70% PA6, the domains of the styrenic component attained a spherical shape and did not tend to aggregation (stable morphology). If PA6 formed domains, then the dispersed PA6 domains tended to aggregate and coalesce at long times. Compatibilized ABS and SAN drops, which were very small (micellelike), were stable in the PA6 matrix. However, the opposite situation (very small compatibilized PA6 drops

in the ABS matrix) did not occur. The morphological analysis indicated asymmetric properties of the interface between PA6 and ABS.

Second, the materials in the dry state behaved much more brittle than those in the wet state. The higher ductility of wet PA6 initiated greater plastic deformation in the blends.

Third, the interface between the ABS particles and the PA6 matrix in the 70% PA6/30% ABS blend was the weak part and promoted debonding and void formation. Partly, better interface adhesion yielded to fibrillation in the interphase. After rupturing of the fibrils, microvoids around ABS particles were also formed.

Fourth, the compatibilizer SANMA was only partly concentrated at the interface but was mostly distributed in the form of small domains in the PA6 phase.

The stimulating discussions with J. Meissner and H. C. Öttinger as well as the support of W. Schmidheiny, F. Mettler, and J. Hostettler are gratefully acknowledged. The authors also thank U. Gösele, Director of the Max Planck Institute of Microstructure Physics in Halle, for the possibility of using the 400-kV transmission electron microscope. This work was performed within the International Union of Pure and Applied Chemistry subcommittee "Structure and Properties of Commercial Polymers" (project no.: 2005-023-2-400).

References

1. Utracki, L. A. Commercial Polymer Blends; Chapman & Hall: London, 1998.
2. Weber, M. Macromol Symp 2002, 181, 189.
3. Weber, M.; Heckmann, W.; Goeldel, A. Macromol Symp 2006, 233, 1.
4. Liu, N. C.; Baker, W. E. Adv Polym Technol 1992, 11, 249.
5. Jeon, H. K.; Zhang, J.; Macosko, C. W. Polymer 2005, 46, 12422.
6. Macosko, C. W.; Jeon, H. K.; Hoye, T. R. Prog Polym Sci 2005, 30, 939.
7. Ajji, A.; Utracki, L. A. Polym Eng Sci 1996, 36, 1574.
8. Jafari, S. H.; Pötschke, P.; Stephan, M.; Warth, H.; Alberts, H. Polymer 2002, 43, 6985.
9. Jafari, S. H.; Pötschke, P.; Stephan, M.; Pompe, G.; Warth, H.; Alberts, H. J Appl Polym Sci 2002, 84, 2753.
10. Majumdar, B.; Paul, D. R.; Oshinski, A. J. Polymer 1997, 38, 1787.
11. Takeda, Y.; Paul, D. R. J Polym Sci Part B: Polym Phys 1992, 30, 1273.
12. Pötschke, P.; Paul, D. R. Macromol Symp 2003, 198, 69.
13. Lee, C. W.; Ryu, S. H.; Kim, H. S. J Appl Polym Sci 1997, 64, 1595.
14. Triacca, V. J.; Ziaee, S.; Barlow, J. W.; Keskkula, H.; Paul, D. R. Polymer 1991, 32, 1401.
15. Kitayama, N.; Keskkula, H.; Paul, D. R. Polymer 2000, 41, 8041.
16. Kitayama, N.; Keskkula, H.; Paul, D. R. Polymer 2000, 41, 8053.
17. Kitayama, N.; Keskkula, H.; Paul, D. R. Polymer 2001, 42, 3751.
18. Majumdar, B.; Keskkula, H.; Paul, D. R. Polymer 1994, 35, 5453.
19. Majumdar, B.; Keskkula, H.; Paul, D. R. J Polym Sci Part B: Polym Phys 1994, 32, 2127.
20. Janik, H.; Gaymans, R. J.; Dijkstra, K. Polymer 1995, 36, 4203.
21. Steenbrink, A. C.; Janik, H.; Gaymans, R. J. J Mater Sci 1997, 32, 5505.
22. Majumdar, B.; Keskkula, H.; Paul, D. R. Polymer 1994, 35, 3164.
23. Pressly, T. G.; Keskkula, H.; Paul, D. R. Polymer 2001, 42, 3043.
24. Araújo, E. M.; Hage, E., Jr.; Carvalho, A. J. F. J Appl Polym Sci 2003, 87, 842.
25. Araújo, E. M.; Hage, E., Jr.; Carvalho, A. J. F. J Appl Polym Sci 2003, 90, 2643.
26. Sailer, C.; Handge, U. A. Macromolecules 2007, 40, 2019.
27. Sailer, C.; Handge, U. A. Macromol Symp 2007, 254, 217.
28. Sailer, C.; Handge, U. A. Macromolecules 2008, 41, 4258.
29. van Duin, M.; Machado, A. V.; Covas, J. Macromol Symp 2001, 170, 29.
30. Michler, G. H.; Lebek, W. Ultramikrotomie in der Materialforschung; Hanser: Munich, 2004.
31. Michler, G. H. Electron Microscopy of Polymers; Springer: Berlin, 2008.
32. Masuda, T.; Nakajima, A.; Kitamura, M.; Aoki, Y.; Yamauchi, N.; Yoshioka, A. Pure Appl Chem 1984, 56, 1457.
33. Aoki, Y. Macromolecules 1987, 20, 2208.
34. Altstädt, V.; De Lucca Freitas, L.; Schubert, D. W. Pure Appl Chem 2004, 76, 389.
35. Möginger, B.; Michler, G. H.; Ludwig, H.-C. In Deformation and Fracture Behaviour of Polymers; Grellmann, W.; Seidler, S., Eds.; Springer: Berlin, 2001; p 335.